

Hydrological Simulations in Red River Basin Using Super High Resolution GCM Outputs with Geostatistical Processes

Mukta SAPKOTA*, Toshio HAMAGUCHI, Yoshinobu SATO and Toshiharu KOJIRI

* Graduate School of Engineering, Kyoto University

Synopsis

This study uses a physically-based distributed hydrologic model, Hydro-BEAM to simulate the observed runoff for the Red River Basin, based on the modified GCM precipitation and temperature. Statistical bias correction method is applied to improve the raw GCM. Then adjustment factors at each grid point are estimated from the correction factors found out at observed points using kriging interpolation method. The present result of the study supports bias correction method. Kriging method applied for interpolation has soundly distributed the adjustment factors required to correct the GCM data. Further study will show an improved reproduction of basin level runoff observations with bias corrected GCM input.

Keywords: GCM output, Bias correction, Kriging, Hydrological simulation

1. Introduction

South-east Asia is one of the most frequently affected regions by flood. Many of the cities in these regions are vulnerable to floods due to their geographic locations in floodplains of large rivers (Dutta and Herath, 2004). Hanoi, the capital of Vietnam, is one of such cities, which is located in the Red River delta with average elevation less than 20m and highly vulnerable to flood (Tran et al., 2007). The Red River Delta is one of the largest deltas in Vietnam, seriously threatened by flood (Hansson et al., 2008). The Red River Delta is the area with all the characteristics of a region in distress, i.e., increasing numbers of floods, dense and increasing population and a low land location (Hansson and Ekenberg, 2002; Hansson et al., 2008). The problem has been compounded in recent years by a number of changes, such as environmental degradation, global climate change, sedimentation and degradation of the existing extensive system of dykes (Hansson and Ekenberg,

2002). In order to address these problems, there is need for studying the hydrological system and simulating different extreme events to visualize the probable floods that would exceed the flood control design standards.

However, in the context of developing countries, there is always limited data. GCM (Global Climate Models) data has been used here for simulation to overcome the data limitation.

2. Study Area

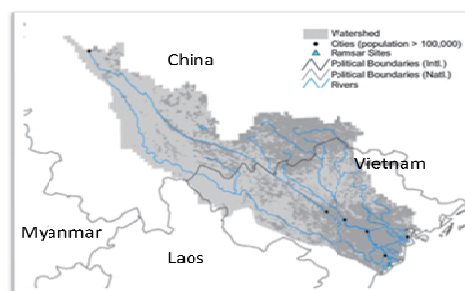


Figure 1. Location map of the Red River Basin

The Red River basin (Fig1) is located in South East Asia (from 20°00 to 25°30 North; from 100°00 to 107°10 East) and drains an area of 156,451 km², of which 50.3% in Vietnam, 48.8% in China and 0.9% in Laos (Le et al., 2007).

3. Methodology

3.1 GCM Data and Bias Correction

GCM data used here is the super high resolution (20km spatial and hourly temporal) GCM outputs based on A1B scenario of IPCC SRES AR4. AGCM20 has been chosen here to bridge the temporal and spatial resolution gap between the GCMs and hydrologic use. Moreover, it has advantage in simulating orographic rainfall and frontal rain bands. Also it has the advantages of avoiding conventional problem on a spatial scale, not requiring further regional or statistical downscaling (Kim et al., 2009 and Kaoru et al., 2009). GCM data used here are precipitation and temperature. However GCMs are often characterized by biases that limit their direct application for basin level hydrological modeling (Sharma et al., 2007). Bias correction method, based on Pearson Type iii distribution, has been applied to improve the raw GCM output. Basic concept behind the data correction is the existence of correlation between GCM outputs, observed and estimated value. The statistical bias correction method used here is based on the initial assumption that both simulated and observed values are well approximated by same probability function as shown in Fig. 2.

Conversion function $f(P_{GCM})$ is determined based on the assumption that the non-exceedance probability of the GCM output is same as that of observed. With this, adjustment factors at each observed point are calculated. Ratio-based and difference-based corrections are applied to precipitation and temperature respectively. Scale factor for precipitation is found out by dividing corrected GCM output by raw GCM output while shift factor for temperature is found out as a difference of corrected GCM output and raw one. Then adjustment factors at each grid points are estimated from the correction factors found out at observed points. For this Kriging interpolation

method is used. This is then applied to get the corrected GCM precipitation and temperature at each grid. Observed daily rainfall from 65 stations for the period of 1979-2000 is used for bias correction for GCM precipitation, while for temperature; observed monthly average temperature from 11 stations for the period of 1996-2000 is used.

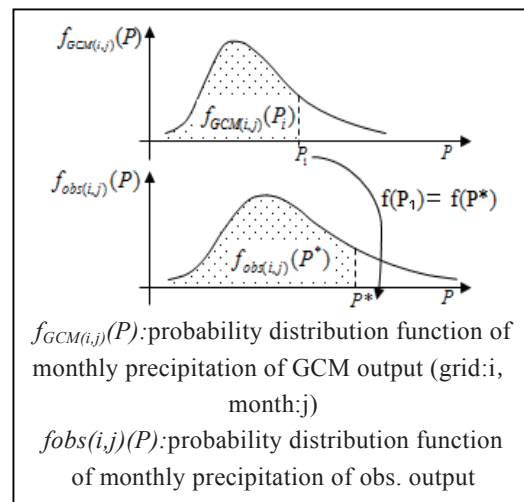


Figure 2. Basic concept of data correction (eg. monthly precipitation)

3.2 Kriging Method for Interpolation

Kriging is an interpolation technique in which the surrounding measured values are weighted to derive a prediction for an unmeasured location. Weights are based on the distance between the measured points, the prediction locations, and the overall spatial arrangement among the measured points. This includes both trend and randomness while interpolating. Various combinations of trend models and covariance models are used to find out the best fit model using Akaike's Information Criterion (AIC). The AIC methodology attempts to find the model that best explains the data with a minimum of free parameters. Covariance models used for the analysis are 1-D and 2-D Spherical, Exponential and Gaussian models. Trend models used are trend in mean, polynomial trends of 1 degree of 1-D of XY axis and 2-D of XY plane.

Adjustment factors from observed stations are distributed using kriging interpolation technique. As there are different models available for kriging method, best fit model is found out using AIC Criterion. Then the same model is used for getting

these factors at each grid point.

3.3 Hydrological Simulation

A physically-based distributed model, Hydro-BEAM (Hydrological River Basin Environment Assessment Model) has been used for rainfall runoff simulation. The model consists of grid cells with DEM and four soil layers (Kojiri et al., 2008). The lateral flow from soil layers A, B and C except D (Fig. 3) can discharge into the river, and the soil moisture can move down and up among the four layers with a no-flux boundary condition at the base of layer D. The model also includes the representation of the hydrologic processes of evapotranspiration, runoff from paddy fields, surface runoff, ground water flow, and flow routing in channel and intake/ release. For considering the variations of infiltration due to the land cover changes, five types of land cover are defined in the model. They are mountainous areas, paddy fields, dry fields, urban lands and water-body surfaces.

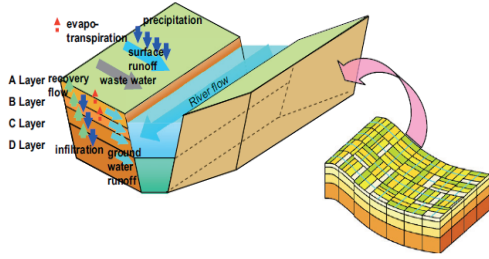


Figure 3. Schematic structure of Hydro-BEAM

Thornthwaite method has been used to calculate potential evapotranspiration in the model as follows:

$$E_p = 0.553D_0 \left(10T_i/J\right)^a \quad (1)$$

$$a = 0.000000675J^3 - 0.0000771J^2 + 0.1792J + 0.049293 \quad (2)$$

$$J = \sum_{i=1}^{12} (T_i/5)^{1.514} \quad (3)$$

$$E_a = M.E_p \quad (4)$$

Where E_p is the potential evapotranspiration at month i (mm/day), and D_0 is the feasible sunshine

duration (h/12 h), a and J are the power index and a heat parameter, and are computed using Equations (2) and (3), respectively. T_i is the monthly averaged temperature at month i ($^{\circ}\text{C}$). E_a is the actual evapotranspiration (mm/day), and M is a parameter for representing available moisture vapor.

Stream routing modeling is done by using the Kinematic wave approximation (Eq. 5 and 6)

$$\frac{\partial h}{\partial t} + \frac{\partial h}{\partial x} = r(x, t) \quad (5)$$

$$q = \alpha h^m \quad (6)$$

Where h is the discharge depth (m), and $r(x, t)$ is the effective rainfall (m/s) at location x and time t . α and m are parameters for computing q .

Surface runoff is calculated using the integrated kinematic wave approximation. This assumes real discharge rate, q_r , to be composed of overland flow rate, q_s , and interflow rate, q_A (Eq. 7).

$$q_r = v_r \cdot h = \begin{cases} q_A & \text{when } h \leq d \\ q_A|h-d + q_s & \text{when } h > d \end{cases} = \begin{cases} \beta h & \text{when } h \leq d \\ \beta h + \alpha(h-d)^m & \text{when } h > d \end{cases} \quad (7)$$

Where, v_r is the velocity of real flow, h is the net depth of water flow, d is net depth of flow in saturation level, α , β and m are parameters for computing q_r .

The linear storage model is used to evaluate the subsurface water in the target area (Eq. 8 and 9)

$$\frac{dS}{dt} = I - O \quad (8)$$

$$O = (k_1 + k_2)S \quad (9)$$

Where, I and O are input and output discharges, respectively. S is storage and k_1 and k_2 are tank coefficients.

Complex tank model has been used to simulate the runoff process in paddy field.

3.4 Data Details

DEM (Digital Elevation models) of 90 m resolution has been used from CGIAR_CSI SRTM database. Land use map of 1 km resolution has been used from GLCC (Global Land Cover Characteristics) data version 2.0. Boundary data of 1 km resolution from HydroSHED has been used.

3.5 Data Preparation

9 km by 9km grid size has been used for the analysis. Longitude and latitude of boundary data were extracted using arc GIS. Boundary for the river basin has been shown in Fig. 4. Flow direction map obtained from DEM has been shown in Fig. 5. GLCC has 24 land use types while in Hydro-BEAM only 5 are considered. Most of the area was found to be forest (61.02 percent) and dry field (31.77 percent). Paddy filed, urban area and water body are found to be 6.54, 0.11 and 0.56 percent respectively. Fig 6 shows the land use distribution.



Figure 4. Red river basin boundary

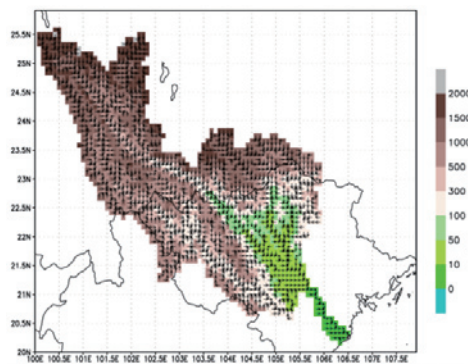


Figure 5. Flow direction map

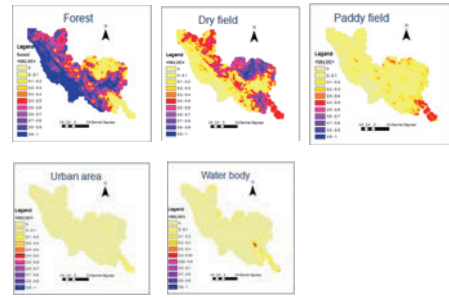


Figure 6. Land use maps

4. Findings and Analysis

4.1 Bias Correction

Bias correction at each observed station for rainfall and temperature is calculated. Results (Fig.7) shows GCM data which over predicts the rainfall scenario for dry season while under predicts the scenario for wet season.

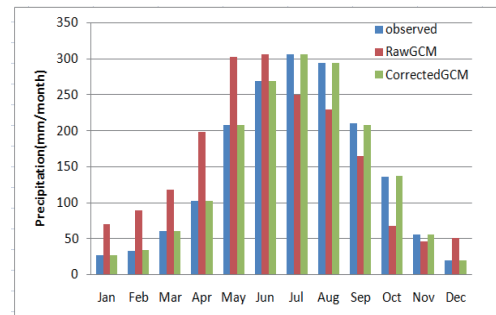


Figure 7. Comparison of observed, raw GCM and bias-corrected GCM (for rainfall)

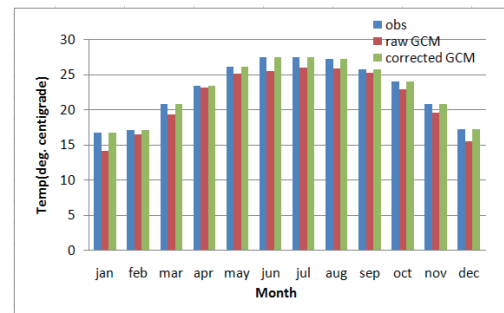


Figure 8. Comparison of observed, raw GCM and bias-corrected GCM (for temperature)

In case of temperature, GCM data is found to be under predicted. Fig 8 can be referred for this.

4.2 Kriging Interpolation

Estimated parameters and evaluated AIC related to different trends and covariance models have been presented in Tables 1, 2 and 3 in the case of

precipitation in January. For January 1-dim spherical model was found out to be suitable.

Similar analyses were done for all months for precipitation and temperature. Table 4 and 5 respectively shows the selected models along with parameters for precipitation and temperature. Then interpolation is done. Scale and shift factor distributions for the month, January have been shown in Figs. 9 and 10 respectively.

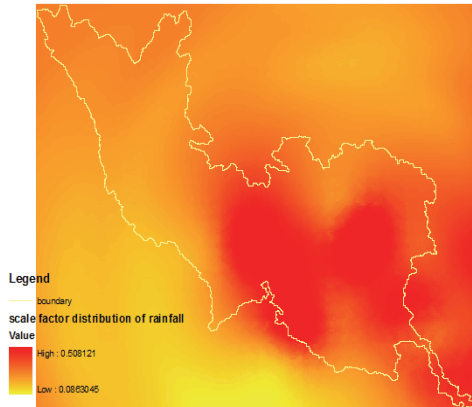


Figure 9. Scale factor distribution (Jan)

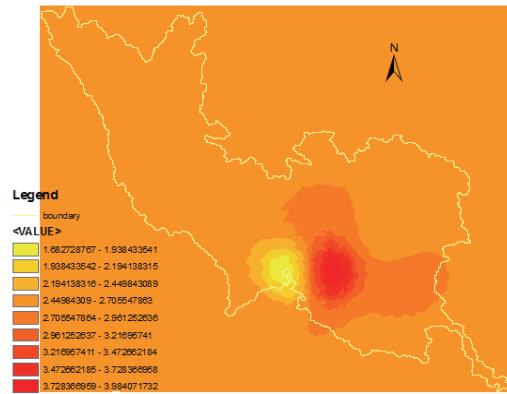


Figure 10. Shift factor distribution (Jan)

In case of precipitation combination of exponential or spherical covariance models with trend function of fixed mean is found to be the best model. While for temperature almost all data best fit in 1-D Spherical models with trend function of fixed mean. Gaussian models are found to be unsuitable in all the cases. The problems of the models are non-convergence or very high value of AIC.

Table 1 Estimated parameters and evaluated AIC related to the trend of b_1 (for precipitation of January)

Covariance fxn model	Trend fxn $m(x)=b_1$	Covariance fxn $C(h)$			MLL	AIC
		σ^2	a_1	a_2		
1-Dim Exponential	3.11E-01	1.33E-02	5.92E-01		2.61E-04	6.001E+00
1-Dim Gaussian						
1-Dim Spherical	2.94E-01	5.59E-02	3.66E+00		1.91E-04	6.000E+00
2-Dim Exponential	3.29E-01	2.30E-04	2.23E-01	4.92E-02	2.19E+03	4.380E+03
2-Dim Gaussian						
2-Dim Spherical	3.29E-01	1.93E-03	8.52E+00	1.31E+00	2.42E+03	4.842E+03

Table 2 Estimated parameters and evaluated AIC related to the trend of $b_1+b_2 R_{xy}$ (for precipitation of January)

Cov. fxn. model	Trend fxn $m(x)=b_1+b_2x+b_3y$			Covariance fxn $C(h)$			MLL	AIC
	b_1	b_2	b_3	σ^2	a_1	a_2		
1-Dim Exponential	-3.16E+00	2.60E-02	3.40E-02	1.25E-02	5.57E-01		2.73E-04	1.00E+01
1-Dim Gaussian								
1-Dim Spherical	-1.10E+01	9.65E-02	5.20E-02	5.48E-02	3.65E+00		2.05E-04	1.00E+01
2-Dim Exponential	1.14E+00	-1.16E-02	1.89E-02	2.20E-04	1.81E-01	4.61E-02	2.13E+03	4.28E+03
2-Dim Gaussian								
2-Dim Spherical	-4.20E+00	4.31E-02	-2.59E-03	1.93E-03	8.54E+00	1.31E+00	2.40E+03	4.82E+03

Table 3 Estimated parameters and evaluated AIC related to the trend of $b_1 + b_2 x + b_3 y$ (for precipitation of Jan)

Covariance fxn. model	Trend fxn $m(x)=b_1+b_2R_{xy}$		Covariance fxn C(h)			MLL	AIC
	b_1	b_2	σ^2	a_1	a_2		
1-Dim Exponential	-2.30E+00	2.42E-02	1.27E-02	5.64E-01		3.76E-04	8.00E+00
1-Dim Spherical	-1.01E+01	9.67E-02	5.52E-02	3.67E+00		1.32E-04	8.00E+00
2-Dim Exponential	2.14E+00	-1.68E-02	2.20E-04	1.89E-01	4.65E-02	2.16E+03	4.33E+03
2-Dim Spherical	-4.47E+00	4.42E-02	1.93E-03	8.54E+00	1.31E+00	2.40E+03	4.82E+03

Table 4 Models chosen for different months and estimated parameters (precipitation)

month	model	Trend fxn	Covariance fxn			MLL	AIC
		$m(x)=b_1$	C(h)				
		b_1	σ^2	a_1	a_2		
jan	1-Dim Spherical	2.94E-01	5.59E-02	3.66E+00		1.91E-04	6.00E+00
feb	1-Dim Spherical	2.93E-01	6.03E-02	4.37E+00		1.74E-04	6.00E+00
mar	1-Dim Spherical	4.09E-01	7.37E-02	4.64E+00		2.29E-04	6.00E+00
apr	1-Dim Exponential	4.75E-01	6.03E-02	1.59E+00		7.86E-05	6.00E+00
may	2-Dim Exponential	7.18E-01	-6.25E-02	-4.18E+01	-2.00E+00	8.17E-05	8.00E+00
jun	1-Dim Exponential	9.49E-01	1.59E-01	4.03E-01		1.62E+01	3.85E+01
jul	2-Dim Exponential	1.25E+00	-1.21E-01	-3.00E+01	-1.79E+00	6.08E-04	8.00E+00
aug	1-Dim Exponential	1.42E+00	2.16E-01	3.22E-01		3.02E+01	6.65E+01
sep	2-Dim Spherical	1.37E+00	-7.89E-02	-2.21E+00	-1.81E+00	1.69E-04	8.00E+00
oct	1-Dim Exponential	2.08E+00	2.00E+00	1.94E-01		1.09E+02	2.24E+02
nov	1-Dim Exponential	1.48E+00	1.15E+01	4.36E-01		1.54E+02	3.14E+02
dec	1-Dim Spherical	2.76E-01	6.06E-02	4.00E+00		1.54E-04	6.00E+00

Table 5 Models chosen for different months and estimated parameters (temperature)

month	model	Trend fxn		Covariance fxn		MLL	AIC
		b_1	b_2	C(h)			
				σ^2	a_1		
jan	1-Dim Spherical	2.65E+00		2.21E+00	5.17E-01	1.92E+01	4.45E+01
feb	1-Dim Spherical	7.49E-01		2.29E+00	5.34E-01	1.94E+01	4.49E+01
mar	1-Dim Spherical	1.21E+02	-1.12E+00	2.78E+00	5.17E-01	2.05E+01	4.90E+01
apr	1-Dim Spherical	2.11E-01		4.09E+00	6.93E-01	2.25E+01	5.10E+01
may	1-Dim Spherical	9.94E-01		1.94E+00	8.28E-01	1.83E+01	4.26E+01
jun	1-Dim Spherical	1.94E+00		1.51E+00	7.89E-01	1.70E+01	3.99E+01
jul	1-Dim Spherical	1.44E+00		1.55E+00	8.74E-01	1.70E+01	4.00E+01
aug	1-Dim Spherical	1.24E+00		1.72E+00	8.16E-01	1.77E+01	4.14E+01
sep	1-Dim Spherical	3.47E-01		2.23E+00	7.76E-01	1.91E+01	4.43E+01
oct	1-Dim Spherical	1.06E+00		2.57E+00	5.21E-01	2.01E+01	4.62E+01
nov	1-Dim Spherical	1.09E+00		2.65E+00	5.29E-01	2.02E+01	4.65E+01
dec	1-Dim Spherical	1.73E+00		2.68E+00	5.09E-01	2.03E+01	4.66E+01

4.3 Hydrological Simulation

Simulation is carried out using the Hydro-BEAM. While calibrating the model, roughness coefficients, peak discharge coefficient and hydraulic conductivity are found to be more sensitive parameters. Further work on calibration is yet to be completed.

5. Conclusions

Bias correction method, based on Pearson Type iii distribution, effectively reduces the biases from raw GCM precipitation and temperature. Kriging method efficiently distributes correction factors at each grid point. AGCM are suitable for hydrological simulation because of its high spatial and temporal resolution. Moreover, the study findings indicate that precipitation and temperature scenarios developed with bias-correction provide an improved reproduction of basin level runoff observations. Further study will come up with a soundly calibrated and validated model which will be able to precisely simulate the discharge at the point of interest.

Acknowledgements

The authors are grateful to the KAKUSHIN Program of the Ministry of Education, Culture, Sports, Science and Technology of Japan (MEXT) for providing the GCM data and Global Center for Education and Research on Human Security Engineering for Asian Megacities for supporting this work.

References

Dutta, D. and Herath, S. (2004): Trends of floods in Asia and Flood Risk Management with Integrated River Basin Approach, Proceedings of the 2nd International Conference of Asia Pacific Hydrology and Water Resources Association,

Singapore, Volume I, pp. 55-63.

Hamaguchi, T. (1998): Studies on inverse problems relating to design for underground dam through new modeling for groundwater flow with moving boundaries, Doctoral dissertation, Kyoto University.

Hansson, K. and Ekenberg, L. (2002): Flood Mitigation Strategies for the Red River Delta, Commons in an Age of Globalisation”, the Ninth Conference, 2002 - dlc.dlib.indiana.edu

Hansson, K., Danielson, M. and Ekenberg, L. (2008): A framework for evaluation of flood management strategies, Journal of Environment Management, Vol. 86, Issue 3, pp. 465-480.

Kaoru, T., Kim, S. Tachikawa, Y. and Nakakita, E. (2009): Assessing Climate Change Impact on Water Resources in the Tone River Basin, Japan, Using Super-High-Resolution Atmospheric Model Output, Journal of Disaster Research Vol. 4, No. 1, pp. 12-23.

Kim, S., Tachikawa, Y., Nakakita, E. and Kaoru, T. (2009): Climate Change Impact on Water Resources Management in the Tone River Basin, Japan, Annuals of Disas. Prev. Res. Inst., Kyoto Univ., No. 52B, pp 587-606.

Kojiri, T., Hamaguchi, T. and Ode, M. (2008): Assessment of global warming impacts on water resources and ecology of a river basin in Japan, J. of Hydro-environment Research, Elsevier, Vol.1, pp.164-175.

Le, T.P.Q., Garnier, J., Gilles, B., Sylvian, T. and Minh, C.V. (2007): The changing flow regime and sediment load of the Red River, Vietnam. Journal of Hydrology, vol. 334, pp. 199-214.

Sharma, D., Gupta, A.D. and Babel, M.S. (2007): Spatial disaggregation of bias-corrected GCM precipitation for improved hydrologic simulation: Ping River Basin, Thailand, Hydrol. Earth Syst. Sci., Vol. 11, No. 4, pp. 1373-1390.

Tran, V.A., Masumoto, S., Raghavan, V. and Shiono, K. (2007): Spatial Distribution of Subsidence in Hanoi Detected by JERS-1 SAR Interferometry, Geoinformatics, vol.18, no.1, pp.3-13.

地球統計学的に処理した超高解像度GCM出力を用いた紅河流域の水文シミュレーション

Mukta SAPKOTA*・浜口俊雄・佐藤嘉展・小尻利治

*京都大学大学院工学研究科

要 旨

本研究は、バイアス補正したGCM(地球大循環モデル)出力の降水量と気温を基にして、ベトナム紅河流域の観測流量をシミュレーションするために分布型水文モデルのHydro-BEAM(流域水文環境評価モデル)を用いる。本稿では、数々のGCMを水文学的に利用する際に存在する時空間的なズレを埋めるため、AGCM20という地球温暖化シナリオを選んだ。ポアソンⅢ型分布を基にしたバイアス補正法を生のGCM出力値の修正に適用している。格子点ごとの補正値は、観測点で算出した補正値からクリギング補間法を用いて空間的に分布推定されている。本稿で示す結果はGCM出力データに使われるバイアス補正法が使えることを示している。空間補間に適用するクリギング法はGCM出力データ補正に必要とされる調整値の空間分布をうまく確実に算出していた。今後は補正されたGCMを入力値として流域の観測流量の再現結果を向上させていく予定である。

キーワード: GCM出力, バイアス補正, クリギング, 水文シミュレーション